POTENTIAL OF X-RAY TOMOGRAPHY FOR THE EXPLORATION OF VEGETAL CONCRETES' POROUS STRUCTURE

M. Lagouin[1]*, P. Sénéchal[2], P. Moonen[2,3], C. Magniont[1], J.E. Aubert[1], A. Laborel-Prénéron[1]

[1] LMDC, Université de Toulouse, INSA, UPS, France
[2] Université Pau & Pays Adour, CNRS, DMEX - IPRA, France
[3] Université Pau & Pays Adour, CNRS, LFCR - IPRA, France

* Corresponding author; e-mail: lagouin@insa-toulouse.fr

Abstract

Vegetal concretes offer promising perspectives as building materials thanks to their low environmental impact and interesting hygrothermal behavior. Their insulating properties and moisture buffering capacity are largely controlled by their microstructure. In this context, X-ray tomography is a promising technique as it enables inner inspection of the microstructure in three dimensions in a non-destructive fashion. Geometrical characteristics, such as the overall porosity and the aggregate volume ratio, can be quantified within the limits of the accuracy of the technique. The present study focuses on a vegetal concrete obtained by combining a metakaolin-based pozzolanic binder with sunflower bark chips. Our measurements show that the vegetal concrete exhibits an open and interconnected pore space, with pore sizes varying over multiple orders of magnitude. The arrangement of the particles is clearly affected by their elongated shape in combination with the compacting force applied during settlement. The material also exhibits shrinkage-induced cracks at the interface between bio-aggregates and binder paste. These observations demonstrate the potential and limitations of X-ray tomography applied to bio-based concretes. The three-dimensional datasets yield more insight compared to typical two-dimensional digital imaging methods such as SEM. Moreover, the non-destructive nature of the method could allow to monitor ageing mechanisms of bio-based concretes by scanning the same sample at different points in time. Similar to other techniques such as SEM, high-resolution tomographic scans can only be obtained on relatively small samples, which raises the question about the representativeness of the specimens in view of the high heterogeneity of vegetal concretes. Nevertheless, the non-destructive nature of the method enables performing multiple scans of different locations within the same sample and to combine the data. X-ray tomography is thus a powerful tool, which can easily be combined with other techniques and contribute to characterize the microstructure of vegetal concretes.

Keywords:

bio-based material, X-ray tomography, porosity, shape parameter, orientation, potential, limitation

1 INTRODUCTION

The growing ecological and environmental consciousness has driven efforts from all sectors to reduce their global environmental footprint. The building industry is particularly concerned as buildings are responsible for approximately 40% of the energy consumption and 36% of the greenhouse gas emissions in the European Union [European Commission 2018]. This sector is the largest consumer of energy, of non-renewable raw materials and the first producer of waste in France [ADEME 2018, Ghewy 2017, SOeS 2016].

These observations have contributed to the rapid development of innovative and sustainable materials. Plant-based building materials are one of them. They are obtained from the processing of agricultural by-products, such as hemp, and have considerable environmental benefits. First, bio-aggregates are derived from an abundant, renewable and vegetal resource which is a carbon sequestration material. Indeed, agricultural products have the property of capturing carbon dioxide from the atmosphere during their growth and storing it into their organisms. Second, the use of plant particles in building materials contributes to the saving of valuable natural resources thanks to agricultural waste recovery [Peñaloza 2016].

Associated with a mineral binder, bio-aggregates enable the design of different types of vegetal concrete. These are hygroscopic materials. Thus, they have the capacity to store or release moisture and, hence, to moderate the daily or seasonal variations of the ambient humidity as well as sudden step changes of the indoor environment [Moujalled 2018]. The low thermal conductivity of vegetal concrete enables to reduce the heat losses in winter and helps to protect against summer heat waves [Tran Le 2010].

Thanks to their ability to manage water vapor transfer and to regulate heat flows, vegetal concretes ensure high indoor environmental quality and contribute to energy saving [Amziane 2017], while limiting the environmental impacts of building materials.

2 MATERIALS AND METHODS

2.1 Materials

Sunflower bark particles

In this study, sunflower bark chips are used as aggregates for an application in vegetal concrete, as they offer interesting characteristics from a microstructural, chemical and physical point of view [Nozahic 2012a, Chabannes 2015]. Furthermore, those particles stem from agricultural by-products available in great quantities on the French territory in general and in the southwest in particular. Sunflower is grown for its seeds, to produce vegetable oil with about 614 000 ha cultivated nationwide, that is to say 230 000 tons of sunflower by-products available each year [GNIS, Laborel-Préneron 2017]. In comparison, despite the fact that hemp shiv is considered as the reference for bio-aggregate, only about 11 000 ha of hemp were cultivated in 2016 in France.

Sunflower bark chips are obtained after harvesting, grinding and mechanical separation. First, stalks are harvested and leaves are pulled off manually directly in fields located in Hautes-Pyrénées (France). Following a drying step, stalks are ground in a hammer mill equipped with a 32 mm diameter grid. In a final phase of separation, a tilted conveyor belt and a blowing system is used to separate the pith from the bark, the two main layers of the stem from the outside to the center of its cross section (Figure 1). Pith is collected in order to produce insulated panels [Sidi Mohamed 2017]. The bark particles are then sieved using a 1 mm grid.

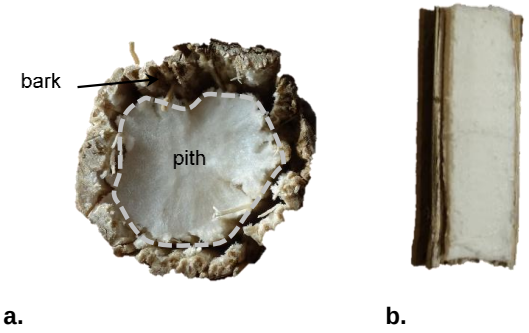

Figure 1 - Structure of sunflower stem: (a) cross-section and (b) longitudinal section

Sunflower composite design, manufacturing and properties

The sunflower concrete employed in the study is formulated with a metakaolin-based pozzolanic binder. Metakaolin is a pozzolanic admixture mainly composed of quartz, silicon and aluminium oxides with an amorphous silico-aluminate mineralogical form. It is produced by flash calcination of kaolinite at 700°C. As all pozzolanic materials, metakaolin reacts in the presence of water with calcium hydroxide to form a binding material. Thus, to formulate the binder, local metakaolin is combined with a commercial slaked lime in proportions determined to optimize binding properties [Dinh 2014]. To further improve the performance of the composite at early age, potassium sulfate is added (2.9% of the binder weight). K_2SO_4 is a chemical activator that encourages ettringite formation and accelerates the pozzolanic reaction [Dinh 2014]. Moreover, a super-plasticizer is introduced in water to improve the mortar workability (1.65% of the water weight). Table 1 summarizes the mix proportions of the Metakaolin-Sunflower (MS) concrete.

Table 1 - Mix design of MS composite

Binder (kg)	Aggregate (kg)	Water (kg)	W/B	A/B
374.3	161.9	371.7	0.99	0.43

A procedure of blending is applied as follows:

- the bark is put in the mixer, water is added for pre-wetting, and the blend is mixed for 2 minutes;
- the anhydrous components are introduced and mixing water with superplasticizer is added. The blend is mixed until a homogeneous mixture is obtained;
- finally, the mold is filled by 3 layers which are compacted by vibratory compaction.

Concretes are manufactured in cylindrical molds that are 11 cm in diameter and 22 cm in length. The mold is removed in two phases. 7 days after concrete pouring, the mold at both ends is removed. 48 days later, samples are completely demolded. The specimens are then stored at ambient room conditions. After curing, resin injection under vacuum is performed to enable extraction of smaller samples for further analysis without losing cohesion (Figure 2).

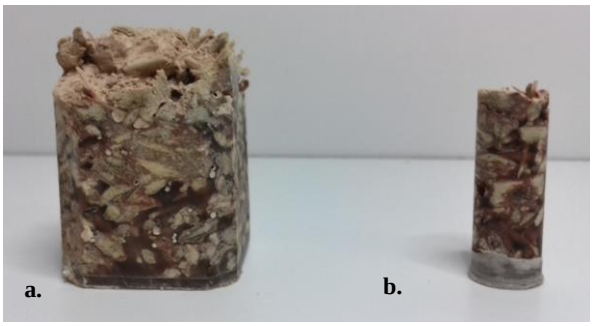

Figure 2 - Sunflower-based samples (a) prismatic sample with a base of 2.33 x 2.33 cm^2 and (b) cylindrical sample with a diameter of 8.8 mm.

2.2 Methods

X-ray tomography acquisition

X-ray tomography is a technique [Banhart 2008], which enables detailed inner inspection of a scanned object in a non-destructive fashion. The sample is placed between a source and a detector. During an acquisition, a conical X-ray beam illuminates the sample and a series of 2D projection images are recorded for various sample orientations. The pixel values of each of these images correspond to the intensity of the transmitted X-ray beam and depend on the attenuation of the sample material. This relationship is expressed by the well-known Beer-Lambert law:

$$I = I_0 e^{-\mu h}$$

where I_0 is the incident X-ray intensity, I is the intensity remaining after the X-ray passes through a homogeneous sample of thickness h and μ is the linear attenuation coefficient that is function of the density and the atomic number of the sample material.

For non-homogeneous media, the product μh is replaced by a line integral along the X-ray path, yielding:

$$I = I_0 e^{-\int_0^h \mu(x)dx}$$

In this study, two tomographs are used to conduct the tomographic acquisition. The Bruker SkyScan 1172 is based on geometric magnification. It features a source having a tunable energy level between 30 kVp and 100 kVp and a 12-bit cooled CCD detector capable of acquiring projection images of 4000 x 2664 pixels. The Zeiss Versa 510 features a combination of optical and geometric magnification. It is equipped with a 10 W X-ray source with a tunable energy level between 30 kVp and 160 kVp, and a 16 bit cooled CCD detector capable of acquiring images of 2048 x 2048 pixels.

Different acquisitions have permitted to characterize the sunflower particles and the MS concrete at various resolutions. To characterize the sunflower particles, a voxel size of 0.74 µm was chosen. Three voxel sizes were selected (19.9, 10 and 4 µm) for the MS concrete acquisitions permitting to obtain information at various scales (global concrete structures, arrangement of aggregate in concrete and interfaces between binder paste, aggregate and voids).

The generator was respectively operated at 30 kVp with a voxel size of 0.74 µm for the sunflower particle; at 40 kVp with a voxel size of 4 and 10 µm and at 70 kVp with a voxel size of 19.9 µm for the MS concrete.

The characteristics of the MS concrete specimen are gathered in Table 2.

Table 2 - Specimen characteristics

Voxel size (µm)	Scanned subset (mm³)	Diameter (mm)	Height (mm)
19.9	3767	19.9	12.12
10	619	8.8	10.18
4	49	3.925	4.05

Data processing

The recorded dataset of 2D projection images can be converted into a three-dimensional dataset, where every voxel (i.e. the three-dimensional counterpart of a pixel) corresponds to the average attenuation coefficient of the physical material located at the voxel position. As attenuation coefficients are material-specific, the analysis of the 3D distribution of attenuation coefficients permits distinguishing pores, binder and aggregates and to determine their geometry and spatial distribution inside the sample, as well as their proportions. Data processing and visualization were performed using Avizo 9.0 (FEI).

3 RESULTS

3.1 Microstructure of sunflower particles

Plant particles exhibit a highly porous structure responsible for transporting the sap of the plant. X-ray tomography enables to quantify the size distribution of this porous structure as well as the interconnectivity of the porous network. *Figure 3***Error! Reference source not found.** depicts the three-dimensional reconstruction of a sunflower bark chip and a two-dimensional cross-section through this volume.

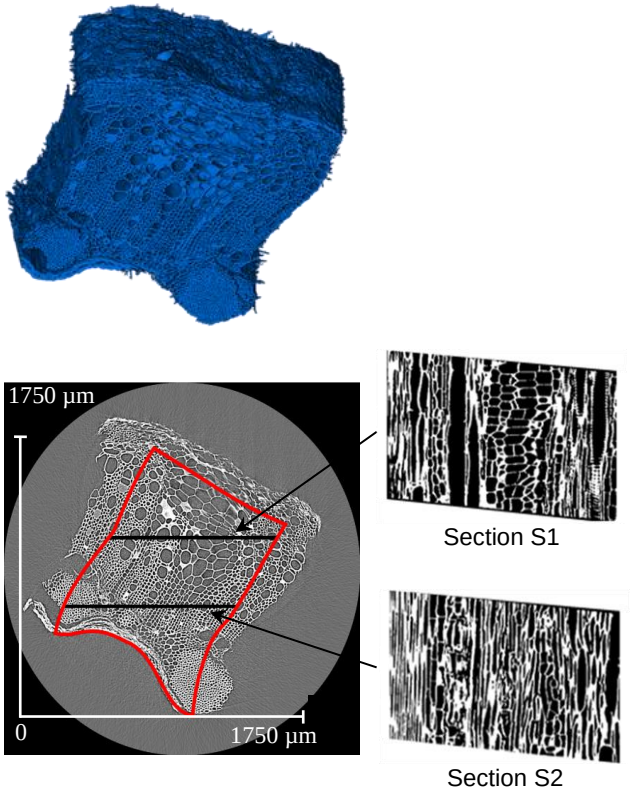

Figure 3 – (a) 3D tomographic reconstruction of a sunflower bark chip, and (b) cross-section through the 3D volume.

A representative volume of the sunflower bark chip is selected (red contour on *Figure 3*b) and its pore structure is qualitatively and quantitatively evaluated.

Analysis revealed both a tubular and alveolar structure. We distinguish alveolar structures with a small diameter (about 60% of pores are below 40 µm in diameter) and vessels with a large diameter (exceeding 100 µm) interconnected throughout the structure.

The average accessible porosity estimated by X-ray tomography is 58 ± 8%. This value appears significantly lower than the disparate and limited results from literature. Mostly obtained by Mercury Intrusion Porosimetry (MIP), gas pycnometry or calculation, the estimated porosity from previous studies for diverse vegetal bark and pith particles ranges from 75 to 99% [Bouasker 2014, Chabriac 2016, Jiang 2017, Jiang 2018, Nozahic 2012b, Rahim 2015, Rahim 2016]. Unlike MIP method which degrades and destructs the particle structures by the application of pressure levels

greater than the compressive modulus of the vegetal particles, X-ray tomography is a non-destructive method which yields an 3D numerical image. However, the obtained porosity value is limited by the scan resolution [Merle 2016]. Indeed, all pores smaller than the resolution (around 3 µm) are not accounted for and therefore porosity is underestimated. Furthermore, the high heterogeneity of the particle could induce important variations of porosity depending on the selected region of interest for analysis.

3.2 Microstructure of MS concrete

In this section, we focus on the different samples of MS concrete. Figure 4 depicts a 2D slice through the scan volume at 4 µm voxel size. It is clear that the differences in grey scale enable proper identification of the different phases: binder paste (light grey), sunflower aggregates (dark grey) and voids (black).

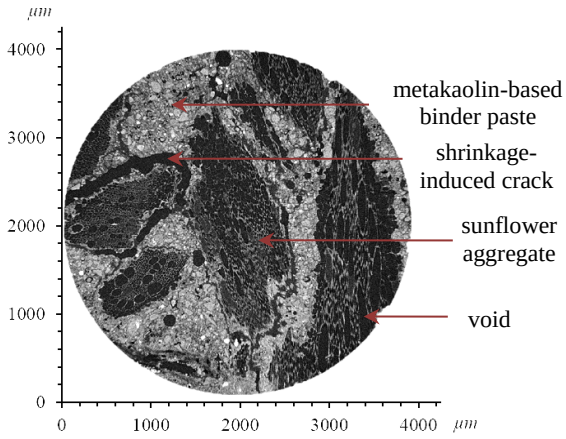

Figure 4 - X-ray tomography slice of MS concrete (voxel size of 4 µm)

The tomographic image also reveals the presence of shrinkage-induced cracks at the interface between the bio-aggregates and the binder paste. Shrinkage happens since the concrete is exposed to a drying environment which causes an increase in tensile stress leading to cracking in absence of external loading [Day 2013]. The shrinkage of concrete is influenced, in particular, by the amount of water present in the fresh concrete: the higher the amount of mixing water is, the greater the drying shrinkage and the resulting occurrence of crack are.

Globally, the vegetal concrete appears highly heterogeneous and exhibits an open and interconnected pore space. These observations are consistent with the work of other authors using different characterization techniques such as vacuum saturation, gas pycnometry and image analysis [Rahim 2016, Cérézo 2005, Chamoin 2013, Collet 2008, Collet 2013, Samri 2008, Evrard 2008, Glé 2011, Gourlay 2017].

Estimation of porosity.

To analyze the porosity in more detail, the tomographic images are segmented into different phases which are subsequently color coded: vegetal particles in green, binder matrix in red and voids in blue (

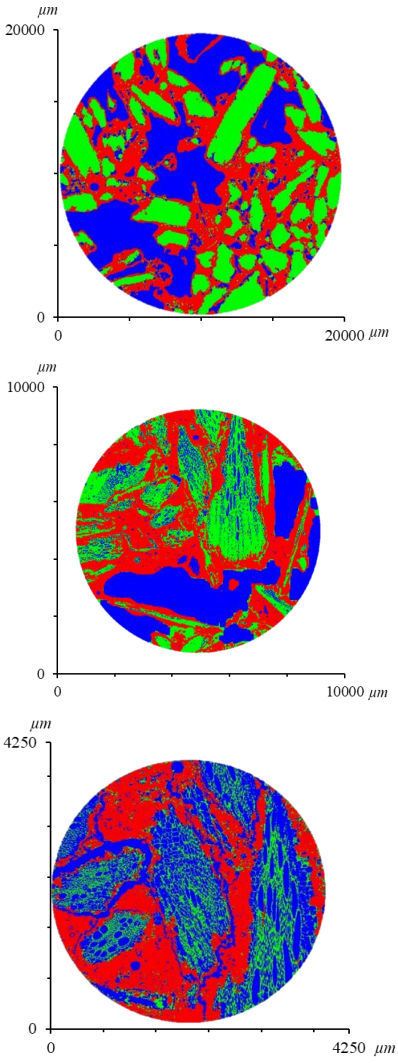

).

Several observations can be made:

- the porosity due to the arrangement between the plant aggregates can reach a millimetric width;
- the porosity due to trapped air in the binder matrix and due to sap vessels in sunflower bark chips shows a width up to 50 µm.
- the nanoporosity due to hydrates arrangement is not detected.

By comparing different resolution images in

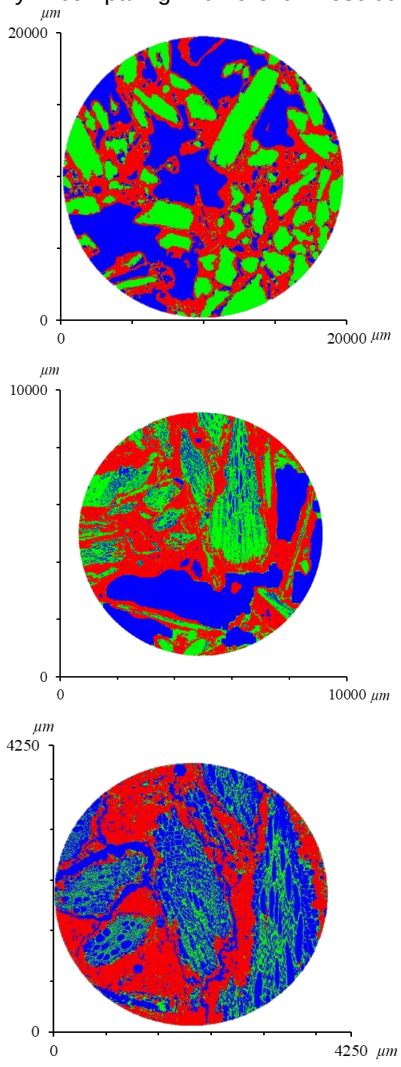

, it logically appears that increasing the scan resolution enables to detect finer pores within the aggregates and binder pastes. Furthermore, the scanned volume decreases with an increase of the resolution. Table 3 summarizes the relative distribution of each phase within the investigated region of interest.

Table 3 - Proportion by volume of each composite phase

Voxel size (µm)	Binder (%)	Aggregates (%)	Void (%)
19.9	37.0	29.7	33.3
10	41.2	30.1	28.7
4	40.6	12.3	47.1

The total porosity (void percentage) obtained in this study cannot be interpreted directly because this quantity depends on the representativeness of the scanned sub volume and varies with the voxel size (linked to the resolution). However, the combination of results obtained at different resolutions can help the interpretation. The largest scanned volume (voxel size of 19.9 µm) is most certainly the most representative and enables determining the proportion of binder (around 37%) and large voids (around 33.3%). At this resolution, distinguishing the aggregates and their internal pores is however not possible. The high-resolution analysis of an aggregate (section 3.1) revealed a porosity of 58 ± 8%. This value can be used to separate the "aggregate" contribution into aggregate (12.5%) and intra-particle porosity (17.2%), leading to a total porosity around 50.5%. Depending on the formulation and the method of determination, the porosities reported in literature mostly range between 60 and 80% [Rahim 2016, Cérézo 2005, Chamoin 2013, Collet 2008, Collet 2013, Driss, Evrard 2008, Glé 2011, Gourlay 2017]. This underestimation can be explained by two major factors:

- the great heterogeneity of materials doesn't guaranty the representativeness of the specimen used by different authors;
- the non-detection of voids below the resolution of tomographic images;

The scans at both higher resolutions become increasingly reliable as far as the inter-particle porosity is concerned, yet the small volume of interest implies that these values are not representative for the sample as a whole. Furthermore, at higher resolution, separating the vegetal particles and the resin becomes difficult, as the contrast between the grey levels is insufficient. A certain number of voxels can therefore be assigned to the wrong phase which would bias the analysis. A possible way out is to use a different type of resin or to perform the tomographic analysis at a different energy.

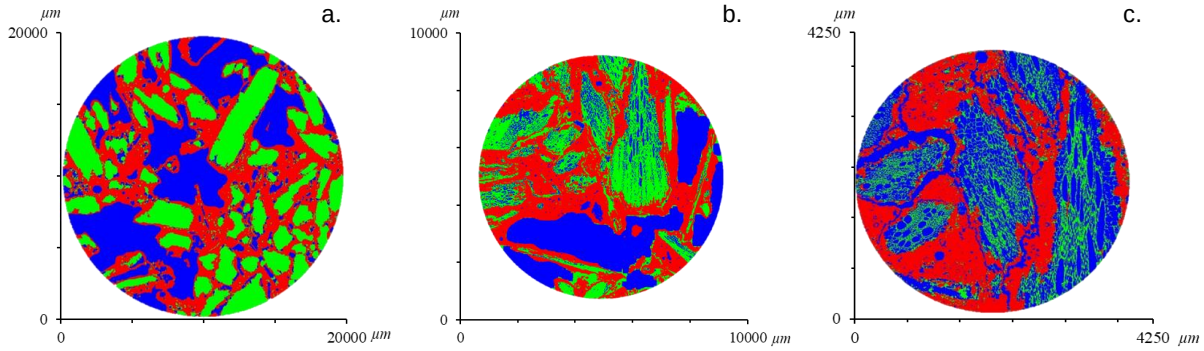

Figure 5 - *Identification of binder (red), aggregate (green) and void (blue) phases in MS composite for three different scan resolutions with voxel sizes of (a) 19.9 µm, (b) 10 µm and (c) 4 µm*

Shape parameters and spatial orientation and shape of bio-aggregates

The 19.9 µm voxel size scan allows extracting the sunflower bark chips, enabling determination of the shape and spatial orientation of bio-aggregates within the binder matrix, as shown in Figure 6.

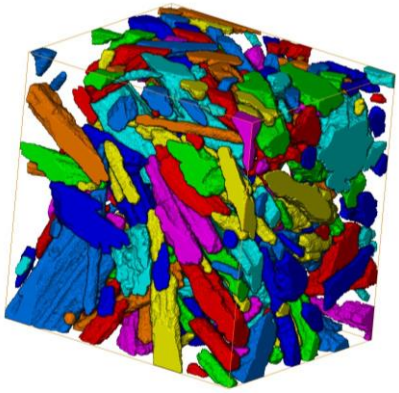

Figure 6 - 3D reconstruction of the sunflower aggregates within the metakaolin binder paste

The geometrical characteristics of the vegetal aggregates within the binder matrix can be calculated by analyzing the eigenvalues of the covariance matrix of each entity. Hereby each bio-aggregate is treated as an ellipsoid (Figure 7a). Three parameters can be defined, namely anisotropy, elongation and flatness:

- the anisotropy is determined as 1 minus the ratio of the minimum over the maximum eigenvalue of the covariance matrix (=*1-Z/X*). It quantifies the deviation from a spherical shape. a perfect sphere has an anisotropy of 0;
- the elongation of each particle is defined as the ratio of the medium and the largest eigenvalue of the covariance matrix (=*Y/X*), causing elongated objects to have values close to 0 (a perfect sphere has an elongation of 1);
- the flatness is the ratio of the smallest and the medium eigenvalue of the covariance matrix (=*Z/Y*), which means that flat objects have values close to 0 (a perfect sphere has a flatness of 1).

Analyses conducted on a sample of 399 particles (Figure 7b-dFigure 7 –) shows that the great majority of aggregates are far from spherical: most of them have an anisotropy close to 1 and an elongation close to 0. The flatness values mainly range from 0.4 to 0.7. Thus, the sunflower bark chips employed in the mix on average resemble an elongated prism.

a.

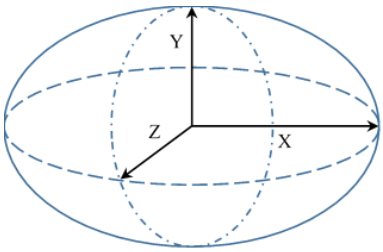

b.

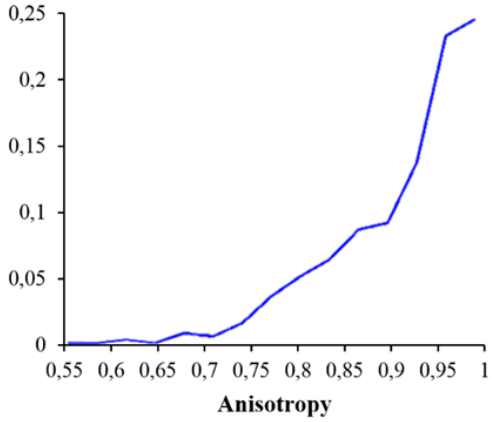

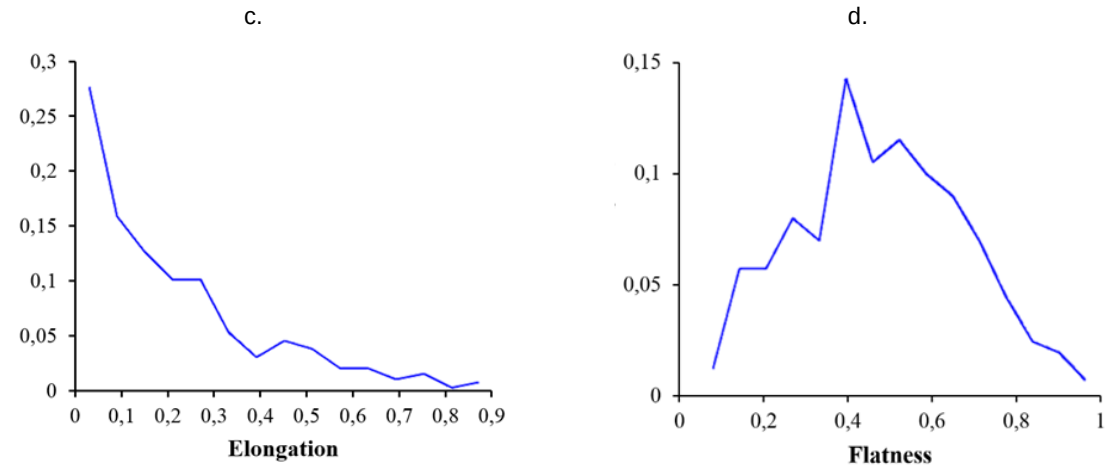

Figure 7 – 399 particles sunflower bark chips are each assimilated to a stress ellipsoid (a) and three shape parameters are calculated and presented as normalized histograms, namely (b) anisotropy, (c) elongation, and (d) flatness.

Next, the spatial orientation of the particles within the metakaolin-based concrete is analyzed. Figure 8 shows the particle inclination with respect to a horizontal plane versus its projected in-plane orientation. The applied convention is schematically depicted in Figure 8b. It is observed that the great majority of aggregates doesn't exhibit a preferential in-plane direction but do show an inclination of less than 40° from the horizontal. This can be attributed to the compaction applied during the casting process directing the elongated particles towards stratified planes transverse to the compaction direction. This observation is in line with previous works [Williams 2018, Williams 2016].

The anisotropic internal arrangement of vegetal concretes is known to give rise to anisotropic physical properties. Some works have underlined the impact of bio-aggregates orientation on thermal and mechanical properties [Hustache 2008, Elfordy 2008, Nguyen 2010].

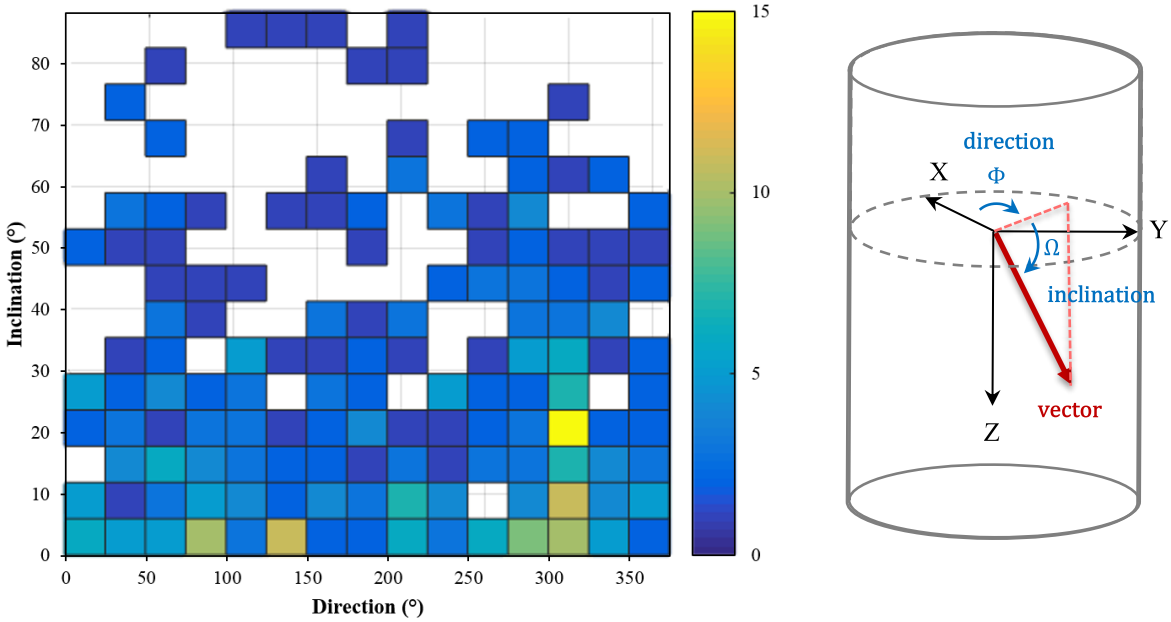

Figure 8 - Spatial orientation of particles: (a) 2d normalized histogram of direction versus inclination and (b) definition of direction and inclination.

4 CONCLUSION

This work is based on the use of a non-destructive technique, X-ray tomography, for the assessment of the internal structure of plant aggregates and bio-based concretes through the application of image analysis.

Evaluation of X-ray tomography images has revealed an open and strongly connected porosity for both sunflower particles and MS concrete. For the sunflower bark chips, the microstructure combines both tubular and alveolar pores. Vegetal concrete was shown to exhibit porosities covering a wide range of scales, from the micrometric size to several millimeters. Furthermore, the presence of shrinkage-induced cracks at the interface between sunflower particles and the metakaolin paste was identified, which are expected to affect the mechanical performance of MS concrete. Furthermore, the arrangement of the particles within MS concrete showed to be clearly affected by their elongated shape in combination with the compacting force applied during settlement, leading to an anisotropic behavior of bio-aggregate materials.

The high heterogeneity of materials questions the representativeness of the specimen. It appears necessary to include a multi resolution analysis to obtain proper results and to take account that the detection of objects smaller than the resolution are not detected.

The use of a resin to solidify the specimen complicates the separation of aggregates with voids. Thus, it seems necessary to harden the composites with a resin either transparent to X-rays or yielding a better contrast. Clearly, the better alternative is avoid the use of resin.

X-ray tomography is thus a powerful tool, which can easily be combined with other techniques and contribute to characterize the microstructure of vegetal concretes. The three-dimensional datasets yield more insight compared to typical two-dimensional digital imaging methods such as SEM. Moreover, the non-destructive nature of the method could allow to monitor ageing mechanisms of bio-based concretes by scanning the same sample at different points in time.

5 REFERENCES

Banhart J. (2008), Advanced Tomographic Methods in Materials Research and Engineering, *Oxford University Press*, 490p. ISBN: 9780199213245.

European Commission (2018), “Buildings - Energy,” *Energy*. [Online]. Available: /energy/en/topics/energy-efficiency/buildings. [Accessed: 30-May-2018].

ADEME (2018), “Qui consomme le plus d’énergie en France ?,” ADEME.

Ghewy X (2017), “Bilan 2014 de la production de déchets en France,” MEEM.

SOeS (2016), “La consommation intérieure de matières en France,” Service de l’Observation et des Statistiques - Ministère de la transistion écologique et solidaire.

Peñaloza D, Erlandsson M, Falk A (2016), “Exploring the climate impact effects of increased use of bio-based materials in buildings,” *Constr. Build. Mater.*, vol. 125, pp. 219–226, doi:10.1016/j.conbuildmat.2016.08.041.

Moujalled B, Aït Ouméziane Y, Moissette S, Bart M, Lanos C, Samri D (2018), “Experimental and numerical evaluation of the hygrothermal performance of a hemp lime concrete building: A long term case study,” *Build. Environ.*, vol. 136, pp. 11–27, doi:10.1016/j.buildenv.2018.03.025.

Tran Le A D, Maalouf C, Mai T H, Wurtz E, Collet F (2010), “Transient hygrothermal behaviour of a hemp concrete building envelope,” *Energy Build.*, vol. 42, no. 10, pp. 1797–1806, doi:10.1016/j.enbuild.2010.05.016.

Amziane S, Collet F (2017), *Bio-aggregates Based Building Materials*, vol. 23. Dordrecht: Springer Netherlands, doi:10.1007/978-94-024-1031-0.

GNIS, “Groupement National Interprofessionnel des Semences et plants,” *Gnis*. [Online]. Available: http://www.gnis.fr/. [Accessed: 20-Dec-2017].

Laborel-Préneron A, Magniont C, Aubert J-E (2017), “Characterization of Barley Straw, Hemp Shiv and Corn Cob as Resources for Bioaggregate Based Building Materials,” *Waste Biomass Valorization*, doi:10.1007/s12649-017-9895-z.

Nozahic V, Amziane S, Torrent G, Saïdi K, De Baynast H (2012a), “Design of green concrete made of plant-derived aggregates and a pumice–lime binder,” *Cem. Concr. Compos.*, vol. 34, no. 2, pp. 231–241, doi:10.1016/j.cemconcomp.2011.09.002.

Chabannes M, Nozahic V, Amziane S (2015), “Design and multi-physical properties of a new insulating concrete using sunflower stem aggregates and eco-friendly binders,” *Mater. Struct.*, vol. 48, no. 6, pp. 1815–1829, doi:10.1617/s11527-014-0276-9.

Sidi Mohamed A, Sabathier V, Evon P, Magniont C, Labonne L (2017), “Contribution to the design and the characterization of a fully bio-based insulated panel including sunflower pith,” presented at the 2nd International Conference on Bio-based Building Materials & 1st Conference on ECOlogical valorisation of GRAnular and FIbrous materials, Clermont-Ferrand, France.

Dinh T M (2014), “Contribution au développement de béton de chanvre préfabriqué utilisant un liant pouzzolanique innovant.”

Bouasker M, Belayachi N, Hoxha D, Al-Mukhtar M (2014), “Physical Characterization of Natural Straw Fibers as Aggregates for Construction Materials Applications,” *Materials*, vol. 7, no. 4, pp. 3034–3048, doi:10.3390/ma7043034.

Chabriac P A, Gourdon E, Gle P, Fabbri A, Lenormand H (2016), “Agricultural by-products for building insulation: Acoustical characterization and modeling to predict micro-structural parameters,” *Constr. Build. Mater.*, vol. 112, pp. 158–167, doi:10.1016/j.conbuildmat.2016.02.162.

Jiang Y, Ansell M, Jia X, Hussain A, Lawrence M (2017), "Physical characterisation of hemp shiv: Cell wall structure and porosity."

Jiang Y, Lawrence M, Ansell M P, Hussain A (2018), "Cell wall microstructure, pore size distribution and absolute density of hemp shiv," *R. Soc. Open Sci.*, vol. 5, no. 4, p. 171945, doi:10.1098/rsos.171945.

Nozahic V (2012b), "Vers une nouvelle démarche de conception des bétons de végétaux lignocellulosiques basée sur la compréhension et l'amélioration de l'interface liant/végétal: application à des granulats de chenevotte et de tige de tournesol associés à un liant ponce/chaux," Université Blaise Pascal-Clermont-Ferrand II.

Rahim M, Douzane O, Tran Le A D, Promis G, Laidoudi B, Crigny A, Dupre B, Langlet T (2015), "Characterization of flax lime and hemp lime concretes: Hygric properties and moisture buffer capacity," *Energy Build.*, vol. 88, pp. 91–99, doi:10.1016/j.enbuild.2014.11.043.

Rahim M, Douzane O, Tran Le A D, Promis G, Langlet T (2016), "Characterization and comparison of hygric properties of rape straw concrete and hemp concrete," *Constr. Build. Mater.*, vol. 102, pp. 679–687, doi:10.1016/j.conbuildmat.2015.11.021.

Merle J, Sénéchal P, Guerton F, Moonen P, Trinsoutrot P, Birot M, Charrier-El Bouhtoury F (2016), "Microstructural characterization of biobased carbon foam by means of X-ray microtomography and compared to conventional techniques," *RSC Adv.*, vol. 6, no. 98, pp. 96057–96064, doi:10.1039/C6RA16969D.

Hustache Y, Arnaud L (2008), "Synthèse des connaissances sur les bétons et mortiers de chanvre."

Cérézo V (2005), "Propriétés mécaniques, thermiques et acoustiques d'un matériau à base de particules végétales: approche expérimentale et modélisation théorique."

Chamoin J (2013), "Optimisation des propriétés (physiques, mécaniques et hydriques) de bétons de chanvre par la maîtrise de la formulation," INSA de Rennes.

Collet F, Bart M, Serres L, Miriel J (2008), "Porous structure and water vapour sorption of hemp-based materials," *Constr. Build. Mater.*, vol. 22, no. 6, pp. 1271–1280, doi:10.1016/j.conbuildmat.2007.01.018.

Collet F, Chamoin J, Pretot S, Lanos C (2013), "Comparison of the hygric behaviour of three hemp concretes," *Energy Build.*, vol. 62, pp. 294–303, doi:10.1016/j.enbuild.2013.03.010.

Samri D (2008), *Analyse physique et caractérisation hygrothermique des matériaux de construction : approche expérimentale et modélisation numérique*. .

Evrard A (2008), "Transient hygrothermal behaviour of Lime-Hemp Materials," p. 142.

Glé P, Gourdon E, Arnaud L (2011), "Acoustical properties of materials made of vegetable particles with several scales of porosity," *Appl. Acoust.*, vol. 72, no. 5, pp. 249–259, doi:10.1016/j.apacoust.2010.11.003.

Gourlay E, Glé P, Marceau S, Foy C, Moscardelli S (2017), "Effect of water content on the acoustical and thermal properties of hemp concretes," *Constr. Build. Mater.*, vol. 139, pp. 513–523, doi:10.1016/j.conbuildmat.2016.11.018.

Driss S, "Analyse physique et caractérisation hygrothermique des matériaux de construction : approche expérimentale et modélisation numérique," p. 285.

Williams J, Lawrence M, Walker P (2018), "The influence of constituents on the properties of the bio-aggregate composite hemp-lime," *Constr. Build. Mater.*, vol. 159, pp. 9–17, doi:10.1016/j.conbuildmat.2017.10.109.

Williams J, Lawrence M, Walker P (2016), "A method for the assessment of the internal structure of bio-aggregate concretes," *Constr. Build. Mater.*, vol. 116, pp. 45–51, doi:10.1016/j.conbuildmat.2016.04.088.

Elfordy S, Lucas F, Tancret F, Scudeller Y, Goudet L (2008), "Mechanical and thermal properties of lime and hemp concrete ('hempcrete') manufactured by a projection process," *Constr. Build. Mater.*, vol. 22, no. 10, pp. 2116–2123, doi:10.1016/j.conbuildmat.2007.07.016.

Nguyen T T, Picandet V, Carre P, Lecompte T, Amziane S, Baley C (2010), "Effect of compaction on mechanical and thermal properties of hemp concrete," *Eur. J. Environ. Civ. Eng.*, vol. 14, no. 5, pp. 545–560, doi:10.1080/19648189.2010.9693246.

Day K W, Aldred J, Hudson B (2013), *Concrete mix design, quality control and specification*. CRC Press.